JOURNAL OF THERMOPHYSICS AND HEAT TRANSFER
Vol. 20, No. 3, July–September 2006

State-to-State Catalytic Models, Kinetics, and Transport in Hypersonic Boundary Layers

I. Armenise*
IMIP/CNR, 70126 Bari, Italy
M. Barbato†
SUPSI-DTI-ICIMSI, 6928 Manno, Switzerland
M. Capitelli‡
Bari University, 70126 Bari, Italy
and
E. Kustova§
Saint Petersburg State University, 198504, Saint Petersburg, Russia

A new iterative model has been developed that couples, in the boundary layer of a reentering body, the equations for N_2, N, O_2, O, and NO mass fractions, N_2 and O_2 vibrational distributions, and gas temperature with the surface state-to-state heterogeneous recombination coefficients has been developed. Results for SiO_2 and metallic surfaces are presented and discussed. The non-Boltzmann behavior of the vibrational distribution functions near the surface is found, as well as the nonmonotonic behavior of the NO density profile along the boundary layer coordinate. The transport coefficients and the heat flux to the surface are calculated using the Chapman–Enskog theory. A strong dependence of transport coefficients and energy flux on the vibrational–chemical kinetics in the boundary layer is shown. In particular, the diffusion coefficients of the first and last vibrational levels differ by several orders of magnitude, according to the shape of vibrational distributions, and the surface material noticeably influences diffusion coefficients of N and NO.

Nomenclature

A^*	=	adatoms density
C_s	=	mass fraction of species s: ρ_s/ρ
C_v	=	ρ_v/ρ
c_{N}, c_{O}	=	constants
D_{cvdw}	=	diffusion coefficients of the vth vibrational level of the species c in the wth vibrational level of the species d, $\mathrm{m}^2 \cdot \mathrm{s}^{-1}$
D_{N}	=	diffusion coefficient of nitrogen atoms in the mixture, $\mathrm{m}^2 \cdot \mathrm{s}^{-1}$
D_{O}	=	diffusion coefficient of oxygen atoms in the mixture, $\mathrm{m}^2 \cdot \mathrm{s}^{-1}$
D_{Tcv}	=	thermal diffusion coefficient of chemical species c in the vibrational level v, $\mathrm{m}^2 \cdot \mathrm{s}^{-1}$
d_{cv}	=	diffusion driving forces, m^{-1}
d_{N}, d_{O}	=	atom diameter, m
E_i	=	the activation energy of the ith process
$E_{a\mathrm{N}_2}$, $E_{a\mathrm{O}_2}$, $E_{a\mathrm{NO}}$	=	adsorption activation energy
$E_{\mathrm{N-N}}$, $E_{\mathrm{O-O}}$, $E_{\mathrm{N-O}}$	=	bond energy between A and B atoms in the molecule, KJ/mol
f	=	stream function
h	=	Planck constant
k	=	Boltzmann constant, $\mathrm{J} \cdot \mathrm{K}^{-1}$
$k_{\mathrm{ch}}^{\mathrm{N}}$, $k_{\mathrm{ch}}^{\mathrm{O}}$	=	chemisorption rate constants, $\mathrm{m}^3 \cdot \mathrm{sites}^{-1} \cdot \mathrm{s}^{-1}$
$k_{\mathrm{chdm}}^{\mathrm{N}_2}$, $k_{\mathrm{chdm}}^{\mathrm{O}_2}$, $k_{\mathrm{chdm}}^{\mathrm{NO}}$	=	chemisorption of diatomic molecules rate constants, $\mathrm{m}^5 \cdot \mathrm{sites}^{-2} \cdot \mathrm{s}^{-1}$
$k_{\mathrm{ER}}^{\mathrm{NN}}$, $k_{\mathrm{ER}}^{\mathrm{OO}}$, $k_{\mathrm{ER}}^{\mathrm{NO}}$, $k_{\mathrm{ER}}^{\mathrm{ON}}$	=	Eley–Rideal recombination rate constants, $\mathrm{m}^3 \cdot \mathrm{sites}^{-1} \cdot \mathrm{s}^{-1}$
k_f	=	pseudo-first-order gas-phase NO formation rate, s^{-1}
$k_{\mathrm{LH}}^{\mathrm{NN}}$, $k_{\mathrm{LH}}^{\mathrm{OO}}$, $k_{\mathrm{LH}}^{\mathrm{NO}}$	=	Langmuir–Hinshelwood recombination rate constants, $\mathrm{m}^2 \cdot \mathrm{part}^{-1} \cdot \mathrm{s}^{-1}$
$k_{\mathrm{td}}^{\mathrm{N}}$, $k_{\mathrm{td}}^{\mathrm{O}}$	=	thermal desorption rate constants, s^{-1}
m_{N}	=	atomic nitrogen mass, kg
m_{O}	=	atomic oxygen mass, kg
N	=	$N_{\mathrm{vibr}} + N_{\mathrm{at}}$
N_{at}	=	number of atomic species
N_{vibr}	=	total number of vibrational states in the mixture
n	=	total mixture number density, $\mathrm{part} \cdot \mathrm{m}^{-3}$
n_{cv}	=	number density of molecules c in the vibrational level v, $\mathrm{part} \cdot \mathrm{m}^{-3}$
$P_{\mathrm{ER}}^{\mathrm{NN}}$, $P_{\mathrm{ER}}^{\mathrm{OO}}$, $P_{\mathrm{ER}}^{\mathrm{NO}}$, $P_{\mathrm{ER}}^{\mathrm{ON}}$	=	steric factor of E–R recombination
P_{N_2}, P_{O_2}, P_{NO}	=	adsorption steric factor
$P_{0r\mathrm{NN}}$, $P_{0r\mathrm{OO}}$, $P_{0r\mathrm{NO}}$, $P_{0r\mathrm{ON}}$	=	E–R microprobability
Pr	=	Prandtl number
p	=	pressure, $\mathrm{N} \cdot \mathrm{m}^{-2}$
$Q_{a\mathrm{N}}$, $Q_{a\mathrm{O}}$, $E_{\mathrm{N-M}}$, $E_{\mathrm{O-M}}$, E_5	=	atom-surface bond energy, KJ/mol
$Q_{\mathrm{ER}}^{\mathrm{NN}}$, $Q_{\mathrm{ER}}^{\mathrm{OO}}$, $Q_{\mathrm{ER}}^{\mathrm{NO}}$, $Q_{\mathrm{ER}}^{\mathrm{ON}}$	=	activation energy of E–R recombination, KJ/mol
$Q_{\mathrm{LH}}^{\mathrm{NN}}$, $Q_{\mathrm{LH}}^{\mathrm{OO}}$, $Q_{\mathrm{LH}}^{\mathrm{NO}}$, E_4	=	activation energy of L–H recombination
q	=	heat flux, $\mathrm{W} \cdot \mathrm{m}^{-2}$
q_{DVE}	=	heat flux due to diffusion of vibrational energy transferred by excited molecules, $\mathrm{W} \cdot \mathrm{m}^{-2}$

Received 15 June 2005; revision received 28 July 2005; accepted for publication 1 August 2005.

*Researcher, Via Amendola 122/D; iole.armenise@ba.imip.cnr.it.
†Senior Researcher, Via Cantonale Galleria 2; maurizio.barbato@supsi.ch.
‡Full Professor, Chemistry Department and IMIP-CNR, Via Orabona 4; mario.capitelli@ba.imip.cnr.it. Associate Fellow AIAA.
§Full Professor, Department of Mathematics and Mechanics, Universitetsky pr. 28; elena_kustova@mail.ru.

q_F = heat flux due to thermal conductivity (Fourier flux), $W \cdot m^{-2}$
q_{MD} = heat flux due to mass diffusion, $W \cdot m^{-2}$
q_{TD} = heat flux due to thermal diffusion, $W \cdot m^{-2}$
S_T = source term of the energy equation
S_v = source terms of the continuity equations
S_0 = the number of active sites per unit area, sites $\cdot m^{-2}$
S_{0N}, s_{0O} = steric factors
Sc = Schmidt number
s_N, s_O = sticking coefficients
T = temperature, K
$T_{e,vib}$ = edge vibrational temperature, K
T_{0N}, T_{0O}, T_{0N_2}, T_{0O_2}, T_{0NO} = threshold temperature, K
V_{cv} = diffusion velocity of species c in the vibrational level v, $m \cdot s^{-1}$
v, w = species indeces
$\bar{\alpha}_{rNN}$, $\bar{\alpha}_{rOO}$, $\bar{\alpha}_{rNO}$, $\bar{\alpha}_{rON}$ = steric factors
β_N, β_O = exponential coefficients for atoms adsorption
β_{N_2}, β_{O_2}, β_{NO} = exponential coefficients for dissociative adsorption
β_{rNN}, β_{rOO}, β_{rNO}, β_{rON} = exponential coefficients for Eley–Rideal recombination
γ_{OO}, γ_{NN}, γ_{ON}, γ_{NO} = recombination coefficients of different surface reactions
Δ = mean distance between sites, m
ε^c = formation energy of species c, J
$\langle \varepsilon^{cv} \rangle_{rot}$ = mean rotational energy, J
ε_v^c = vibrational energy of the level v of the species c, J
η = coordinate normal to the surface
Θ = T/T_e
θ = surface coverage, non dimensional
λ_{TR} = thermal conductivity coefficient of translational and rotational degrees of freedom, $Kg \cdot m \cdot K^{-1} \cdot s^{-3}$
ρ = total density, $kg \cdot m^{-3}$
ρ_v = density in the vth vibrational level, $kg \cdot m^{-3}$
ρ_N, ρ_{N_2}, ρ_O, ρ_{O_2}, ρ_{NO} = N, N_2, O, O_2, and NO density, $kg \cdot m^{-3}$

Subscripts

e = external edge of the boundary layer
w = wall

Superscript

$*$ = active adsorption site

I. Introduction

CATALYTIC heating effects are of paramount importance in the modeling and simulation of reentry problems. In fact, for the flight trajectory segments characterized by large values of Mach number, diffusion and recombination of atomic species on the surface can represent a consistent part of the total heat flux. The assumption of a noncatalytic surface can lead to strong underestimation of the thermal load to the vehicle thermal protection systems (TPS), the reverse being true for the assumption of fully catalytic behavior of the vehicle surface. Adequate catalyticity models must be therefore developed and inserted into computational fluid dynamics tools to realize accurate estimates of vehicle surface heating, with the final goal of helping TPS designers both in the design phase and in the postflight data analysis.

For the reentry vehicle TPS, the coating material has to show poor catalytic properties to reduce as much as possible the energy released at the surface by catalytic reactions. For the range of temperatures experienced by this class of vehicles, even a small difference in catalycity can make a large difference in the heat load. For this reason, the hypersonic community has been strongly interested in this topic since the 1950s.[1–4]

Several experimental studies on high-energy flows near body surfaces have made available data on recombination probabilities (i.e., ratios between the number of atoms recombined at the surface and the total number of atoms impinging on the surface).

The pioneering work of Greaves and Linnet[1] was the first source of data for hypersonic applications. The experimental studies of Halpern and Rosner for metal surfaces[4,5] then gave an important contribution, not only by the wide range of temperatures explored and the number of surface materials considered, but also by the important discussions and conclusions they drew about the possibility of incomplete accommodation of the recombination energy. In the 1970s and 1980s, thanks to studies related to the space shuttle, great interest was devoted to the experimental evaluation of the catalytic behavior of materials applicable as surface coatings for TPS tiles. Scott produced arc-jet data for the recombination coefficients on high-temperature reusable surfaces insulation.[6] Stewart et al. performed experiments on space shuttle instrumented tiles to gather in-flight data directly.[7] Several sets of experimental data for reacted cured glass (RCG) were made available from different sources,[8–10] and the large scatter they show is an index of the complexity of the phenomena involved.

The strong temperature dependence shown by the recombination coefficient experimental data and the inadequacy of the noncatalytic and fully catalytic surface models were the main reasons driving the study of finite-rate-catalysis models. The first temperature-dependent models were based on the Arrhenius-like expressions obtained by fitting experimental data.[6,11] With the progress of research, the sophistication of the model was increased and has led to models developed from the physics and chemistry of the elementary mechanisms involved in the heterogeneous processes.[12–16]

From different modeling experiences, a number of lessons have been learned: recombination coefficient models have to include their dependence on surface material, chemical species, and temperature; local characteristics such as gas composition near the wall can affect the recombination probabilities,[17] recombination coefficients calculated for binary mixtures (e.g., N_2–N or O_2–O) cannot be used directly for dissociated air due to the interaction between different atomic species on the catalyst adsorption sites,[14] the catalytic formation of NO,[18] and the coupling of these effects with atomic nitrogen and oxygen catalytic recombination.[14,16,18]

The experimental and theoretical approaches thus far presented must be considered phenomenological approaches because they neglect the possibility of selective pumping of given vibrational levels during the recombination phase. To investigate this point, we need a state-to-state model for microscopic collision kinetics as well as a molecular dynamic approach to give information on the state-to-state rates.

To this end, a state-to-state vibrational model for the interaction of atomic oxygen on SiO_2 in a hypersonic boundary layer has been developed.[19] The SiO_2 material was chosen as a representative of the catalytic behavior of TPS coatings based on RCG.[10] The model treats a heterogeneous recombination process,

$$O + O^* \xrightarrow{\gamma_{OO}} O_2(v) + {}^*$$

that is able to form vibrationally excited molecules selectively in the gas phase.

The relevant rate coefficients were obtained using the molecular dynamic calculation of Cacciatore et al.[20] In the model, the molecules in different vibrational states are considered as different species. The gas-phase kinetics follows the ladder-climbing model.[21,22] In a subsequent paper,[23] these ideas were extended to dissociating air on the same SiO_2 surface. In this case, phenomenological recombination coefficients were taken from the literature.[14] In addition, it was assumed that during the recombination process, all the recombination energy was used to pump the last vibrational level of the relevant molecules (N_2, O_2). Gas-phase elementary processes

then redistribute this energy over the vibrational manifolds of the molecules. In the case of oxygen atoms, this model provides good agreement with the results obtained using the molecular dynamic approach.

The model has recently been improved to take into account, also in the case of dissociating air, state-to-state recombination on the surface.[24]

This phenomenological approach, however, disregards the coupling between different heterogeneous reactions occurring on the surface. A first attempt to overcome this problem has been made in Ref. 25. In this paper, the state-to-state model for a silica surface developed in previous work,[19,23] has been improved to take into account more advanced recombination coefficient models that include dependence on surface material, temperature, and gas composition near the wall, as well as interaction between different atomic species on the catalyst adsorption sites.[14] In particular, this new model couples the flowfield solution with the surface recombination coefficient calculations.

In the present paper, we extensively apply this model to both SiO_2 and metallic surfaces. In addition, we use the results in the calculation of transport coefficients and the heat flux to the vehicle using the Chapman–Enskog theory, including the effect of nonequilibrium vibrational distributions.[26,27]

II. The Model

A. Surface Phenomena

The interaction of dissociated gases, as well as of partially ionized gases, with a solid surface produces a series of heterogeneous phenomena. Different situations, including plasma flows in a tube and high-energy flows past atmosphere re-entry vehicles, as well as past scaled models inside hypersonic wind tunnels, offer examples of this phenomenology. The heterogeneous interaction is due to two simultaneous factors: the presence of dissociated atoms and the existence of dangling chemical bonds on the solid surface. These locations on the surface are called "sites." On these sites gas atoms (or molecules) can be chemically adsorbed (chemisorbed), that is, can form chemical bonds on the surface site, becoming "adatoms." In some cases, the solid surface can promote reactions between adsorbed particles, and gas particles, making available a more favorable energetic path for chemical reactions without directly participating in the chemical reactions. In this case, the solid surface acts as a catalyst,[28] promoting recombination reactions and formation of new chemical species. For the applications connected to this work, the heterogeneous reactions of interest involve O and N atoms that form N_2, O_2, and NO.

The number of active sites per unit area, $[S_0]$, depends on the solid material and can be of the order of 10^{19} sites per square meter. In the general situation, not all the surface sites are occupied by adatoms; therefore the number of unoccupied sites per unit area will be: $[S] = [S_0] - [A^*]$, where $[A^*]$ is the adatom density. The characterization of the level of adatom coverage for a solid surface is usually done by defining a nondimensional parameter called surface coverage:

$$\theta = [A^*]/[S_0]$$

that is, the ratio between the adatom density and the number of active sites per unit area.

In the surface interaction processes studied in this work, the vibrational deactivation has not been included.

The modeling approach to describe the heterogeneous kinetics can be schematically summarized as follows[14,17,28]: 1) diffusion of reactants to the surface; 2) adsorption of reactants at the surface; 3) chemical reaction on the surface; 4) desorption of products from the surface; 5) diffusion of products away from the surface. Usually steps 1 and 5 are assumed to be very fast. For this reason, in the present work, the diffusion steps are not considered, and the primary focus is on the kinetic for the elementary processes 2, 3, and 4.

Let us consider atom and molecule chemisorption. The process involves the adsorption of an atom/molecule (A/M) on an active site * of the surface, forming a so called adatom A^*:

$$\mathrm{N} + {}^* \longrightarrow \mathrm{N}^* \tag{1}$$

$$\mathrm{O} + {}^* \longrightarrow \mathrm{O}^* \tag{2}$$

$$\mathrm{N_2} + 2^* \longrightarrow \mathrm{N}^* + \mathrm{N}^* \tag{3}$$

$$\mathrm{O_2} + 2^* \longrightarrow \mathrm{O}^* + \mathrm{O}^* \tag{4}$$

$$\mathrm{NO} + 2^* \longrightarrow \mathrm{N}^* + \mathrm{O}^* \tag{5}$$

Once formed, adatoms can react with gas-phase atoms, producing molecules according to the Eley–Rideal recombination mechanism:

$$\mathrm{N} + \mathrm{N}^* \longrightarrow \mathrm{N_2} + {}^* \tag{6}$$

$$\mathrm{O} + \mathrm{O}^* \longrightarrow \mathrm{O_2} + {}^* \tag{7}$$

$$\mathrm{N} + \mathrm{O}^* \longrightarrow \mathrm{NO} + {}^* \tag{8}$$

$$\mathrm{O} + \mathrm{N}^* \longrightarrow \mathrm{NO} + {}^* \tag{9}$$

On the other hand, adatoms can react between themselves, forming molecules in the gas phase through the Langmuir–Hinshelwood recombination mechanism:

$$\mathrm{N}^* + \mathrm{N}^* \longrightarrow \mathrm{N_2} + 2^* \tag{10}$$

$$\mathrm{O}^* + \mathrm{O}^* \longrightarrow \mathrm{O_2} + 2^* \tag{11}$$

$$\mathrm{N}^* + \mathrm{O}^* \longrightarrow \mathrm{NO} + 2^* \tag{12}$$

Finally, adatoms can desorb according to the following mechanism:

$$\mathrm{N}^* \longrightarrow \mathrm{N} + {}^* \tag{13}$$

$$\mathrm{O}^* \longrightarrow \mathrm{O} + {}^* \tag{14}$$

The rate constant of each elementary kinetic process (1)–(14) can be expressed in the classical Arrenhius form[14,28] as reported in the Appendix.

Using the classical chemical kinetics theory, one can write the following rate equations for the concentrations of nitrogen [N*] and oxygen [O*] adatoms:

$$\begin{aligned}\frac{\mathrm{d}[\mathrm{N}^*]}{\mathrm{d}t} &= [\mathrm{N}]([S_0] - [\mathrm{N}^*] - [\mathrm{O}^*])k_{\mathrm{ch}}^{\mathrm{N}} + [\mathrm{N_2}]2([S_0] - [\mathrm{N}^*] \\ &\quad - [\mathrm{O}^*])^2 k_{\mathrm{chdm}}^{\mathrm{N_2}} + [\mathrm{NO}]([S_0] - [\mathrm{N}^*] - [\mathrm{O}^*])^2 k_{\mathrm{chdm}}^{\mathrm{NO}} \\ &\quad - [\mathrm{N}][\mathrm{N}^*]k_{\mathrm{ER}}^{\mathrm{NN}} - [\mathrm{O}][\mathrm{N}^*]k_{\mathrm{ER}}^{\mathrm{ON}} \\ &\quad - 2[\mathrm{N}^*][\mathrm{N}^*]k_{\mathrm{LH}}^{\mathrm{NN}} - [\mathrm{N}^*][\mathrm{O}^*]k_{\mathrm{LH}}^{\mathrm{NO}} - [\mathrm{N}^*]k_{\mathrm{td}}^{\mathrm{N}}\end{aligned} \tag{15a}$$

$$\begin{aligned}\frac{\mathrm{d}[\mathrm{O}^*]}{\mathrm{d}t} &= [\mathrm{O}]([S_0] - [\mathrm{N}^*] - [\mathrm{O}^*])k_{\mathrm{ch}}^{\mathrm{O}} + [\mathrm{O_2}]2([S_0] - [\mathrm{N}^*] \\ &\quad - [\mathrm{O}^*])^2 k_{\mathrm{chdm}}^{\mathrm{O_2}} + [\mathrm{NO}]([S_0] - [\mathrm{N}^*] - [\mathrm{O}^*])^2 k_{\mathrm{chdm}}^{\mathrm{NO}} \\ &\quad - [\mathrm{O}][\mathrm{O}^*]k_{\mathrm{ER}}^{\mathrm{OO}} - [\mathrm{N}][\mathrm{O}^*]k_{\mathrm{ER}}^{\mathrm{NO}} - 2[\mathrm{O}^*][\mathrm{O}^*]k_{\mathrm{LH}}^{\mathrm{OO}} \\ &\quad - [\mathrm{N}^*][\mathrm{O}^*]k_{\mathrm{LH}}^{\mathrm{NO}} - [\mathrm{O}^*]k_{\mathrm{td}}^{\mathrm{O}}\end{aligned} \tag{15b}$$

where $[S_0]$, as already stated, is the initial concentration of active sites.

The system of equations can be solved under stationary conditions using the Newton–Raphson method.

At this stage, it is clear that the surface processes, depending also on the molecular and atomic fluxes on the surface itself, affect the numbers of both nitrogen and oxygen adatoms per unit area. On the other hand, the number of adatoms per unit area enters into the expressions for the recombination coefficients, which in turn affect the heterogeneous dissociation–recombination surface

reactions, and therefore the concentrations of the species in the gas phase.

The heterogeneous dissociation–recombination reactions included in the present model are

$$N + N^* \xrightarrow{\gamma_{NN}} N_2(v) + * \tag{16}$$

$$O + O^* \xrightarrow{\gamma_{OO}} O_2(v) + * \tag{17}$$

$$O + N^* \xrightarrow{\gamma_{ON}} NO + * \tag{18}$$

$$N + O^* \xrightarrow{\gamma_{NO}} NO + * \tag{19}$$

and the corresponding recombination coefficients defined in Refs. 14 and 28,

$$\gamma_{AB} = \frac{\text{Flux of atoms recombining at the surface}}{\text{Flux of atoms impinging on the surface}} \tag{20}$$

are obtained by simple considerations.

On one hand, considering N_2, O_2, NO dissociation–recombination, the expressions

$$-\frac{d[N]}{dt} = 2\frac{d[N_2]}{dt} + \frac{d[NO]}{dt} \tag{21a}$$

$$-\frac{d[O]}{dt} = 2\frac{d[O_2]}{dt} + \frac{d[NO]}{dt} \tag{21b}$$

hold for the [N] and [O] time variations.

On the other hand, the $[N_2]$, $[O_2]$, [NO] time variations due to the surface processes discussed are

$$\frac{d[N_2]}{dt} = -[N_2][S]^2 k_{chdm}^{N_2} + [N][N^*]k_{ER}^{NN} + [N^*]^2 k_{LH}^{NN} \tag{22a}$$

$$\frac{d[O_2]}{dt} = -[O_2][S]^2 k_{chdm}^{O_2} + [O][O^*]k_{ER}^{OO} + [O^*]^2 k_{LH}^{OO} \tag{22b}$$

$$\frac{d[NO]}{dt} = -[NO][S]^2 k_{chdm}^{NO} + [N][O^*]k_{ER}^{NO} + [O][N^*]k_{ER}^{ON} + [N^*][O^*]k_{LH}^{NO} \tag{22c}$$

The recombination coefficients are therefore (see also Refs. 14 and 28)

$$\gamma_{NN} = \frac{2\left(-[N_2][S]^2 k_{chdm}^{N_2} + [N][N^*]k_{ER}^{NN} + [N^*]^2 k_{LH}^{NN}\right)}{Z_N} \tag{23a}$$

$$\gamma_{OO} = \frac{2\left(-[O_2][S]^2 k_{chdm}^{O_2} + [O][O^*]k_{ER}^{OO} + [O^*]^2 k_{LH}^{OO}\right)}{Z_O} \tag{23b}$$

$$\gamma_{NO} = \frac{-[NO][S]^2 k_{chdm}^{NO} + [N][O^*]k_{ER}^{NO} + [O][N^*]k_{ER}^{ON} + [N^*][O^*]k_{LH}^{NO}}{Z_N} \tag{23c}$$

$$\gamma_{ON} = \frac{-[NO][S]^2 k_{chdm}^{NO} + [N][O^*]k_{ER}^{NO} + [O][N^*]k_{ER}^{ON} + [N^*][O^*]k_{LH}^{NO}}{Z_O} \tag{23d}$$

where $Z_A = [A]\sqrt{(kT/2\pi m_A)}$, with $A = N, O$.

B. Boundary Layer Equations and Chemical Kinetics

The elementary heterogeneous processes discussed in the previous section have been inserted into the boundary layer equations to investigate the combined effect of both gas-phase and surface processes on the flow properties.

To stress the roles of both the gas-phase vibrational processes and the surface ones, the fluid dynamics has been kept as simple as possible: the simplest flow (axisymmetric or unlimited in one direction) has been chosen, the stagnation point approximation[29,30] has been used, and a two-dimensional system has been reduced to the following one-dimensional system of boundary layer equations:

$$C_v'' + f \cdot Sc \cdot C_v' = S_v \tag{24a}$$

$$\Theta'' + f \cdot Pr \cdot \Theta' = S_T \tag{24b}$$

using the Lees-Dorodnitsyn transformations[29] (see also Chaps. 5 and 6 of Ref. 30) in the self-similar reference system. Equations (24a) are continuity equations of the concentrations of the 46 vibrational levels of N_2, of the 33 vibrational levels of O_2, of N and O atoms, and of NO molecules, the last ones considered without detailing the internal structure. The last assumption, which simplifies the calculations, is mainly due to the poor knowledge of the relevant state-to-state rate coefficients involving NO(v). Equation (24b) is the energy equation. The source terms S_v and S_T include state-to-state nonequilibrium vibrational kinetics for N_2 and O_2 (including dissociation and recombination processes[21,22]) according to the ladder-climbing model as well as NO formation chemical reactions[21]:

vv (vibration–vibration energy exchange):

$$N_2(v) + N_2(w) \leftrightarrow N_2(v-1) + N_2(w+1) \tag{25}$$

$$O_2(v) + O_2(w) \leftrightarrow O_2(v-1) + O_2(w+1) \tag{26}$$

vTm (vibration–translation energy exchange involving molecules):

$$N_2(v) + N_2 \leftrightarrow N_2(v-1) + N_2 \tag{27}$$

$$O_2(v) + O_2 \leftrightarrow O_2(v-1) + O_2 \tag{28}$$

vTa (vibration-translation energy exchange involving atoms):

$$N_2(v) + N \leftrightarrow N_2(w) + N \tag{29}$$

$$O_2(v) + O \leftrightarrow O_2(v-1) + O \tag{30}$$

and exchange reactions:

$$N_2(v) + O \leftrightarrow NO + N \tag{31}$$

$$N_2(A) + O \rightarrow NO + N(^2D) \tag{32}$$

where $N_2(A)$ and $N(^2D)$ are respectively molecules in the excited electronic state

$$A \equiv {}^3\sum_u^+$$

and atoms in the excited electronic state ^2D. Because of energy considerations, the $N_2(A)$ state concentration is assumed to be equal to the concentration of the ground state

$$N_2\left({}^1\sum_g^+\right)$$

level $v = 25$, as reported in Ref. 23.

The rate coefficients of processes (27)–(32) are reported in Refs. 21–23.

Finally, in Eqs. (24a) and (24b), the Prandtl and Schmidt numbers have been approximated to the constant values of $Pr = 0.71$ and $Sc = 0.49$.

The assumption of a constant Schmidt number for diffusion is a simplification, which is however consistent with the simplified fluid dynamics used in the present work. We are conscious that the surface catalytic heating is controlled by the mass flux of atoms, which in turn depends on the choice of a model for the mass transport. The use of one-dimensional boundary layer equations, including multicomponent diffusion coefficients, could improve the final results, avoiding the uncorrect assumption of constant Prandtl and Schmidt numbers. This point is under study in our laboratory.

C. Finite Rate Catalysis Boundary Conditions

At the edge of the boundary layer thermal and chemical equilibrium is assumed; therefore, a single equilibrium temperature T_e is introduced to describe translational and internal degrees of freedom. Vibrational level populations follow the Boltzmann distribution with temperature T_e. It is interesting that a boundary layer edge vibrational temperature $T_{e,\mathrm{vib}}$ not equal to T_e would lead to different results.[24]

The gas temperature near the surface is assumed to be equal to the wall temperature T_w. One should keep in mind that in the general case, the temperature jump can influence the temperature distribution near catalytic surfaces. In the present study this effect is neglected in order to avoid further model complications.

Other surface boundary conditions necessary for solving Eqs. (24), are the conditions for species derivatives, which take into account surface processes described by Eqs. (16–19):

$$\left.\frac{\partial C_{\mathrm{N}}}{\partial \eta}\right|_w = \frac{\sum_v \gamma_{\mathrm{NN}}(v)}{D_{\mathrm{NN}}}\sqrt{\frac{kT}{2\pi m_{\mathrm{N}}}}\cdot C_{\mathrm{N}} + \frac{\gamma_{\mathrm{NO}}}{D_{\mathrm{NN}}}\sqrt{\frac{kT}{2\pi m_{\mathrm{N}}}}\cdot C_{\mathrm{N}} \quad (33a)$$

$$\left.\frac{\partial C_{\mathrm{N}_2}(v)}{\partial \eta}\right|_w = -\frac{\gamma_{\mathrm{NN}}(v)}{D_{\mathrm{NN}}}\sqrt{\frac{kT}{2\pi m_{\mathrm{N}}}}\cdot C_{\mathrm{N}} \quad (33b)$$

$$\left.\frac{\partial C_{\mathrm{O}}}{\partial \eta}\right|_w = \frac{\sum_v \gamma_{\mathrm{OO}}(v)}{D_{\mathrm{OO}}}\sqrt{\frac{kT}{2\pi m_{\mathrm{O}}}}\cdot C_{\mathrm{O}} + \frac{\gamma_{\mathrm{ON}}}{D_{\mathrm{OO}}}\sqrt{\frac{kT}{2\pi m_{\mathrm{O}}}}\cdot C_{\mathrm{O}} \quad (33c)$$

$$\left.\frac{\partial C_{\mathrm{O}_2}(v)}{\partial \eta}\right|_w = -\frac{\gamma_{\mathrm{OO}}(v)}{D_{\mathrm{OO}}}\sqrt{\frac{kT}{2\pi m_{\mathrm{O}}}}\cdot C_{\mathrm{O}} \quad (33d)$$

$$\left.\frac{\partial C_{\mathrm{NO}}}{\partial \eta}\right|_w = -\frac{\gamma_{\mathrm{ON}}}{D_{\mathrm{OO}}}\sqrt{\frac{kT}{2\pi m_{\mathrm{O}}}}\cdot C_{\mathrm{O}} - \frac{\gamma_{\mathrm{NO}}}{D_{\mathrm{NN}}}\sqrt{\frac{kT}{2\pi m_{\mathrm{N}}}}\cdot C_{\mathrm{N}} \quad (33e)$$

It should be noted that the recombination coefficients γ for molecular species calculated according to Eqs. (21–23) use the coefficients k from the catalytic model in Refs. 14 and 28 (see also the Appendix). These coefficients are indeed used in Eqs. (33) by spreading them,[24] in analogy with a state-to-state molecular dynamics approach, into the different vibrational levels. A better model could probably be developed by more efficiently coupling the catalysis, described by molecular dynamics methods, with the nonequilibrium vibrational kinetics.

The diffusion coefficients D_{NN} and D_{OO} are calculated in the code on the basis of the modified Chapman–Enskog theory[26,31] (see Sec. II.E). In our previous study (see Refs. 19, 23–25 and 27) we used constant values of diffusion coefficients for the definition of surface recombination rates. Comparison of the heat flux in the boundary layer calculated using correct diffusion coefficients with the corresponding heat flux obtained in our previous work gives differences up to 30%.

D. Numerical Method

Details of the numerical method, which is a finite difference one, can be found in the literature.[19,21–23] Here we only discuss the main modifications of the model.

It should be noted that the coordinate normal to the surface, η, is divided into 80 nodes, this choice being reasonable in light of the χ^2 test performed on the basis of the "grid convergence" numerical experiments reported in Ref. 25. Note also that to discretize Eqs. (24) on this grid, central finite differences have been used.

The solution method is an iterative one, which also includes the calculation of both the recombination coefficients γ and the diffusion coefficients D to be used in the boundary conditions (33).

At each iteration

1) The concentrations computed by the previous iteration are used to evaluate the diffusion coefficients (see Sec. II.E) to be inserted in the boundary conditions (33)

2) The same concentrations are used to evaluate the nitrogen and oxygen adatom concentrations [Eq. (15)]

3) The updated adatom concentrations are then used to calculate the recombination coefficients γ for all the molecular species [see Eqs. (23)]

4) The updated values of both diffusion coefficients D and recombination coefficients γ are inserted into the finite-rate catalysis boundary conditions [see Eqs. (33)]

5) The equations system (24) is discretized and solved to update the concentrations

6) The process is then repeated from 1 to 5 until the concentrations converge.

The iterative process is described in Figs. 1a–1c for typical reentry conditions characterized by the following parameters for the edge of the boundary layer and for the surface: $T_e = 7000$ K, $P_e = 1000$ N/m^2, $T_w = 1000$ K (SiO_2 surface). In particular, Fig. 1a

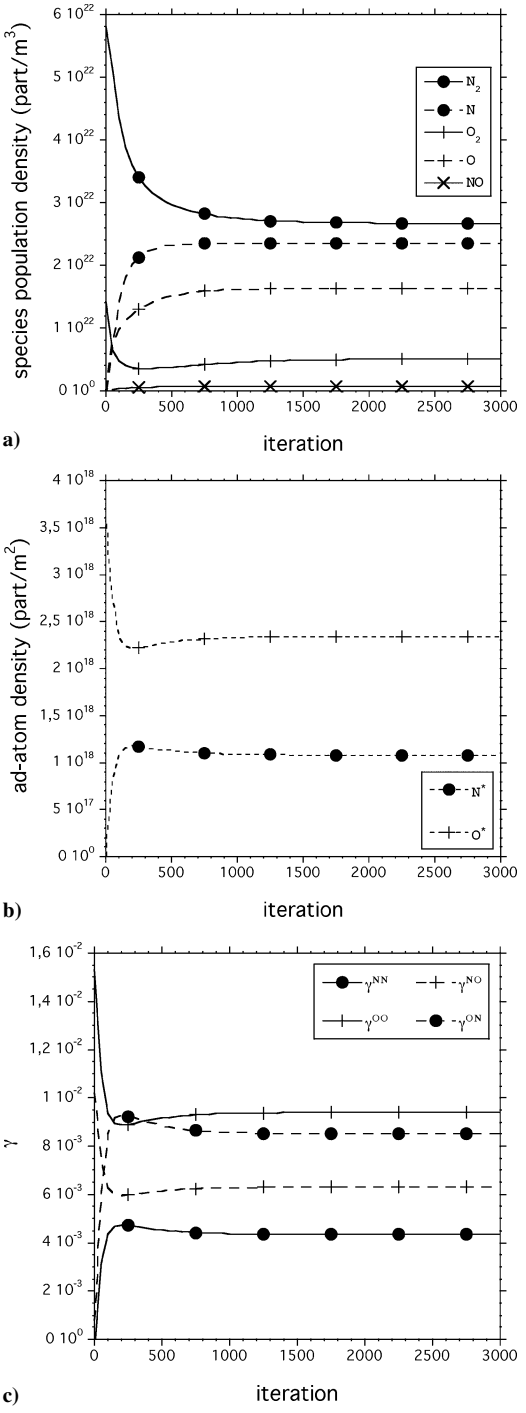

Fig. 1 Gas species population densities over the surface (a), adatom densities (b), and recombination coefficients (c) for a SiO_2 surface.

reports the N_2, N, O_2, O, and NO population densities near the surface, Fig. 1b gives the N^* and O^* densities, and Fig. 1c presents the recombination coefficients of different heterogeneous processes as functions of the iteration number. The results reported in the figure show the mutual influence of the flowfield (represented by the surface population densities) and the surface (represented by the concentrations of N^* and O^* adatoms and the recombination coefficients). To better understand the results, we recall that the initial conditions of our problem correspond to thermal and chemical equilibrium along the initial temperature profile, which linearly decreases from $T_e = 7000$ K to $T_w = 1000$ K. This means that at the first iteration, only N_2 and O_2 molecules exist, while the concentration of O^* adatoms strongly exceeds that of N^* due to the fact that at 1000 K, a fraction of O_2 molecules are dissociated and can therefore be chemiadsorbed by the surface. The change of the considered variables during the iterative process is due to the diffusion of different species across the boundary layer. Of course, only the values corresponding to the last iteration have a physical meaning for the selected boundary conditions.

E. State-to-State Transport Model

For accurate evaluation of the heat flux to the surface, an appropriate model of transport properties taking into account detailed vibration–chemical kinetics both in the gas phase and on the surface should be applied. A theoretical approach to the calculation of state-to-state transport coefficients was developed in Refs. 26 and 31 on the basis of the modified Chapman–Enskog theory. This model shows that the heat flux is determined in this case by the gradients of temperature, pressure, and all vibrational-level populations. The following expression for the heat flux has been derived in the state-to-state approach:

$$q = -\lambda_{TR}\nabla T - p\sum_{c,v}(D_{Tcv}d_{cv}) + \sum_{c,v}\left(\frac{5}{2}kT + \langle\varepsilon^{cv}\rangle_{\rm rot} + \varepsilon_v^c + \varepsilon^c\right)n_{cv}V_{cv} \tag{34}$$

where λ_{TR} is the thermal conductivity coefficient of translational and rotational degrees of freedom, D_{Tcv} is the thermal diffusion coefficient for each vibrational level v of chemical species c, n_{cv} is the number density of molecules c at the vibrational level v, $\langle\varepsilon^{cv}\rangle_{\rm rot}$ is the mean rotational energy, ε_v^c and ε^c are the vibrational energy of the level v and energy of formation of species c, and d_{cv} are the diffusion driving forces. In a flow along the stagnation line, when the pressure is assumed to be constant across the boundary layer, diffusion driving forces depend only on the gradients of vibrational level populations:

$$d_{cv} = \nabla(n_{cv}/n)$$

(n is the total mixture number density). The diffusion velocity for each vibrational state v of species c is defined as

$$V_{cv} = -\sum_{d,w}(D_{cvdw}d_{dw}) - D_{Tcv}\nabla\ell_n T \tag{35}$$

D_{cvdw} are the diffusion coefficients for each vibrational state and chemical species. The total amount of diffusion coefficients is of the order of $N^2 (N = N_{\rm vibr} + N_{\rm at}$, where $N_{\rm vibr}$ is the total number of vibrational states in the mixture and $N_{\rm at}$ is the number of atomic species).

Following the procedure developed in Refs. 26 and 31, the transport coefficients can be found as solutions of linear transport systems and thus expressed in terms of the bracket integrals depending on the cross sections of elastic collisions and the inelastic ones leading to the change of rotational energy. Moreover, the transport coefficients depend on the temperature, the number densities of species, and all vibrational-level populations of molecular species. This fact causes difficulties for the implementation of the state-to-state transport algorithms in the computational fluid dynamics, because the dimension of transport linear systems is of the order of N. In Ref. 26, some simplifications for the state-to-state transport coefficients were proposed, allowing a significant reduction of the computational time required for their calculation. However, the reduced transport linear systems should be solved in each time and space step of a CFD code. This fact still makes it difficult to implement the state-to-state transport model directly to the numerical solvers.

In the present paper, to evaluate the transport properties, we use an approximate approach proposed earlier in Refs. 32 and 33. First, the flow parameters (vibrational level populations and gas temperature) and their gradients are found as solutions of a simplified problem, Eqs. (24a) and (24b). Then these quantities are used for the transport coefficients, diffusion velocity, and heat flux calculation on the basis of rigorous kinetic theory methods developed in Refs. 26 and 31. This allows one to understand the influence of microscopic collisional processes on the heat transfer and also estimate contributions of various dissipative processes to the total energy flux. Indeed, the total energy flux in the state-to-state approach can be represented as a sum of several contributions:

$$q = q_F + q_{\rm MD} + q_{\rm TD} + q_{\rm DVE} \tag{36}$$

where q_F is the heat flux caused only by thermal conductivity (the Fourier flux),

$$q_F = -\lambda_{TR}\nabla T \tag{37}$$

$q_{\rm MD}$ and $q_{\rm TD}$ are the fluxes caused by mass and thermal diffusion, and $q_{\rm DVE}$ is the flux due to diffusion of vibrational energy transferred by excited molecules. The terms q_F, $q_{\rm MD}$, and $q_{\rm TD}$ appear in all commonly used definitions of the total heat flux (both one-temperature and multitemperature formulations) and depend on the gradients of temperature, pressure, and chemical species molar fractions. The last term, $q_{\rm DVE}$, is a characteristic feature of the state-to-state model; it is determined by the gradients of the vibrational level populations.

Under specific flow conditions, there is a competition between various processes. Thus, in shock-heated gases, the contributions of mass diffusion and heat conduction have opposite signs, whereas in a boundary layer, there is no competition between these processes. The role of diffusion of vibrational energy can be important under conditions of strong vibrational nonequilibrium, for instance, near the surface, where the vibrational distributions are far from the equilibrium ones.[33] The influence of thermal diffusion on the heat transfer is usually weak compared to the contributions of other dissipative processes.

III. Results for SiO_2 and Metal Surfaces

Let us examine the results obtained for different surfaces.

Note that we have neglected NO Eley–Rideal recombination as well as NO adsorption on the all surfaces due to the poor knowlege of the corresponding rate coefficients in the case of Pt and Ni surfaces.

The relevant mass fractions along η are plotted in Figs. 2a–2e. As expected, concentrations of N_2 and O_2 molecules increase from the edge of the boundary layer to the surface, the reverse being true for N and O atoms. The NO concentration profile shows nonmonotonic behavior because of the strong nonequilibrium character of the N_2 vibrational distribution function, which is responsible for the formation of NO through the gas phase reaction (31). In any case, the metal surfaces show higher catalyticity than the SiO_2 surface. The mass fractions depend on the considered material: the higher-molecular-mass fractions correspond to metal surfaces, the higher-atomic-mass fractions to the SiO_2 surface. This trend is exactly the one we would expect; however, it is slightly different from the trend obtained in Fig. 1 of Ref. 25. This difference is due to 1) the state-to-state surface recombination model adopted here, 2) the diffusion coefficients $D_{\rm NN}$ and $D_{\rm OO}$ in Eqs. (33), which are calculated now in the code itself (and no longer included as fixed parameters), and 3) surface processes considered in the present study and in Ref. 25 (NO chemisorption as well as NO Eley–Rideal recombination has been neglected here).

The vibrational distributions of N_2 and O_2 on different selected surfaces are given in Figs. 3a and 3b. Heterogeneous reactions actively pump vibrational energy into the molecular species formed at

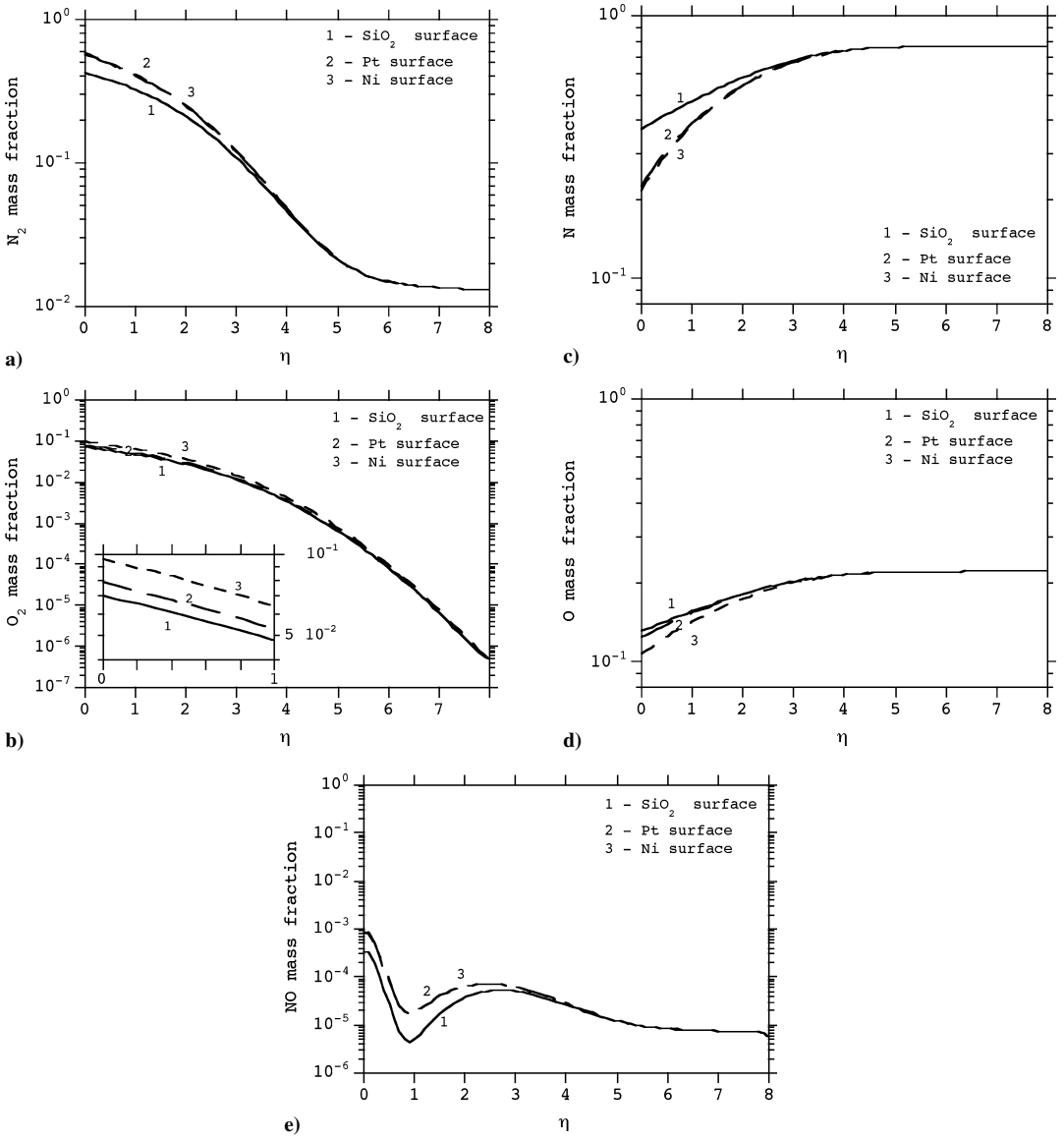

Fig. 2 Mass fractions along η, for different surfaces: a) N_2, b) O_2, c) N, d) O, and e) NO.

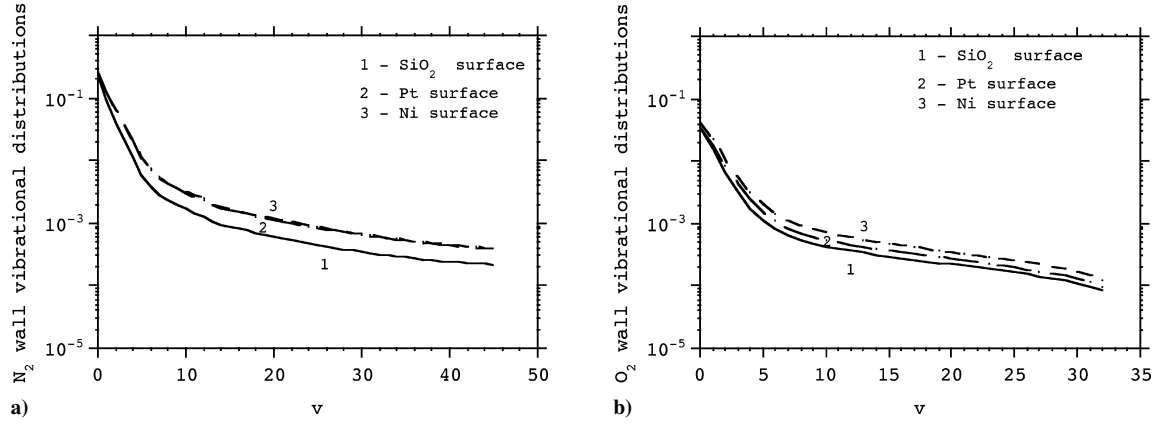

Fig. 3 N_2 (a) and O_2 (b) surface ($\eta = 0$) vibrational distributions vs the vibrational level v for different surfaces.

the surface. Correspondingly, vibrational distributions at the surface show a strong non-Boltzmann character. The Pt and Ni surfaces produce the highest pumped vibrational distributions near the surface because of the higher recombination rate.

The dependence of the mass fractions and of the vibrational distributions near the surface (H = 0) on the different materials follows the catalyticity trend reported in Table 1 for the corresponding recombination coefficients.

Let us now consider the temperature gradients (Fig. 4), which play an important role in the Fourier heat flux calculation. Close to the wall ($\eta < 0.5$), metal surfaces provide a temperature gradient slightly stronger than that obtained for the SiO_2 surface. With increasing distance from the surface ($\eta > 0.5$), an inverse dependence has been obtained.

Now let us discuss the influence of surface material and kinetic surface processes on the transport properties. Thermal diffusion

Table 1 Adatom densities and recombination coefficients on different surfaces obtained by neglecting the NO Eley–Rideal recombination and the NO adsorption

Surface material	N*	O*	γ_{NN}	γ_{OO}	γ_{NO}	γ_{ON}
SiO_2	9.1×10^{17}	3.0×10^{18}	3.7×10^{-3}	1.2×10^{-2}	0	0
	(1.1×10^{18})	(2.3×10^{18})	(4.3×10^{-3})	(9.4×10^{-3})	(6.3×10^{-3})	(8.5×10^{-3})
Pt	4.1×10^{16}	1.2×10^{18}	1.6×10^{-2}	1.4×10^{-2}	7.1×10^{-15}	1.4×10^{-14}
Ni	2.3×10^{17}	1.3×10^{18}	1.7×10^{-2}	2.3×10^{-2}	1.7×10^{-14}	3.9×10^{-14}

Note: $T_e = 7000$ K, $P_e = 1000$ N/m^2, $T_w = 1000$ K; initial mixture composed 79.99975% of nitrogen, 20% of oxygen, 0.00025% of NO. In parentheses are the values obtained using the full heterogeneous recombination model.

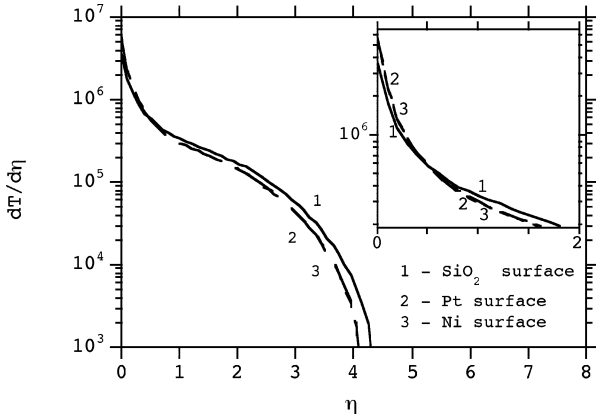

Fig. 4 Temperature gradients vs the normal to the surface η, obtained using different surfaces.

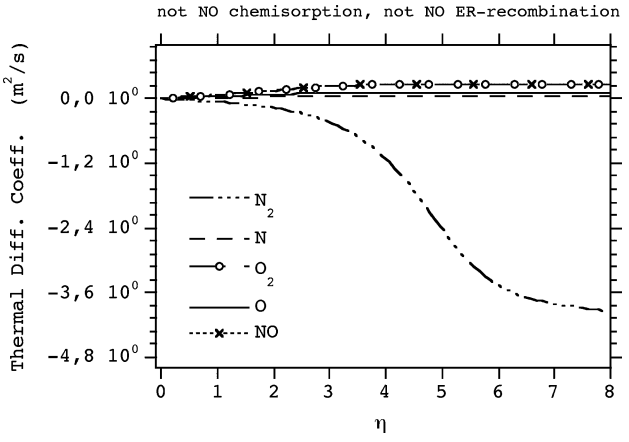

Fig. 5 Species thermal diffusion coefficients along η for a SiO_2 surface.

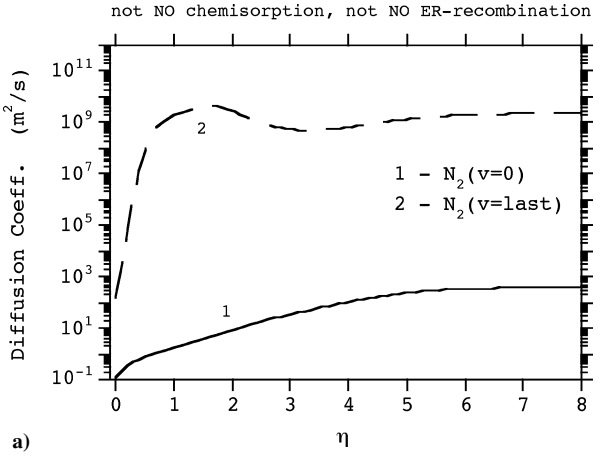

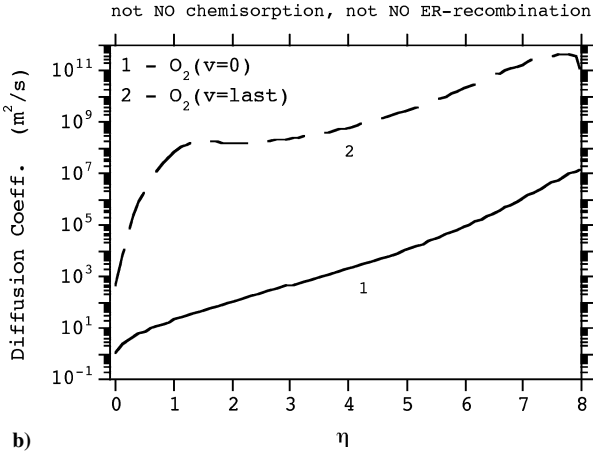

Fig. 6 N_2 (a) and O_2 (b) first and last vibrational level self-diffusion coefficients along η for a SiO_2 surface.

coefficients (Fig. 5), diffusion coefficients (Figs. 6 and 7), thermal conductivity coefficient (Fig. 8a), shear viscosity coefficient (Fig. 8b), Fourier heat flux (Fig. 9a), and total heat flux (Fig. 9b) have been calculated on the basis of the model described in Sec. II.E. Relevant results are plotted in the indicated figures as functions of η.

The thermal diffusion coefficients corresponding to the SiO_2 surface are given in Fig. 5. One can see that thermal diffusion coefficients of O_2, N, O, and NO are positive, whereas for molecular nitrogen the coefficient is negative because[34]

$$\sum_i C_i D_{Ti} = 0$$

Moreover, its absolute value is noticeably higher, especially approaching the external edge of the boundary layer. The influence of the surface material on the thermal diffusion coefficients is found to be weak (except the coefficient D_{TN}; in this case a maximum difference of about 10–30% has been obtained). For all coefficients, the SiO_2 surface provides slightly lower values than the metallic surfaces. This is due to the fact that the temperature calculated for the SiO_2 surface is lower than for other surfaces.

The self-diffusion coefficients of selected vibrational states and chemical species are given in Figs. 6 and 7. Because the dependence of self-diffusion coefficients on the corresponding species molar fraction is close to inverse proportionality, the variation of the coefficients can be rather high. Thus, the diffusion coefficients of the first and last vibrational levels differ by several orders of magnitude (Fig. 6), according to the shape of the vibrational distributions (Fig. 3). The surface material noticeably influences the diffusion coefficients of N and NO; this is probably caused by different rates of NO formation at various surfaces. Indeed, the concentration of O_2 and O is weakly affected by the surface material, whereas the mass fractions of NO and N strongly depend on the surface nature (see Fig. 2).

The trend of thermal conductivity and shear viscosity coefficients (Fig. 8) is the same as the trend of thermal diffusion coefficients. We can conclude that higher recombination rates at metal surfaces cause higher thermal diffusion, thermal conductivity, and shear viscosity coefficients, although the difference is not very strong.

The Fourier flux and the total heat flux are reported in Figs. 9a and 9b. It is seen that the Fourier heat flux follows the temperature

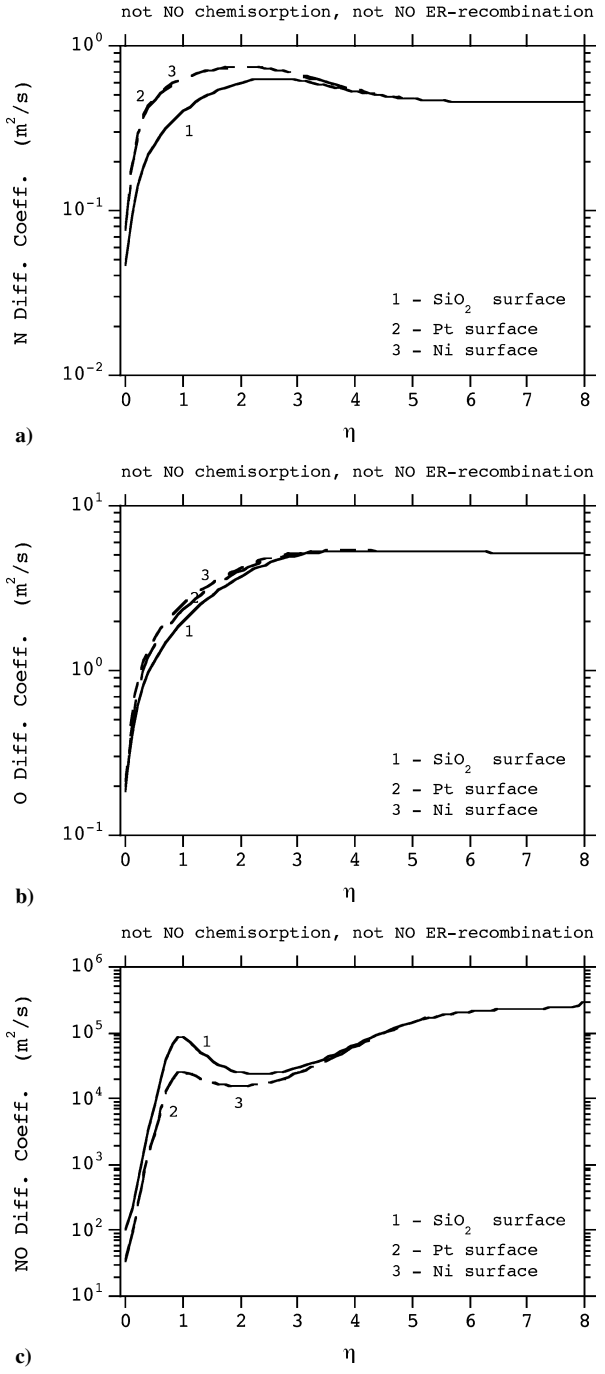

Fig. 7 N (a), O (b), and NO (c) self-diffusion coefficients along η for different surfaces.

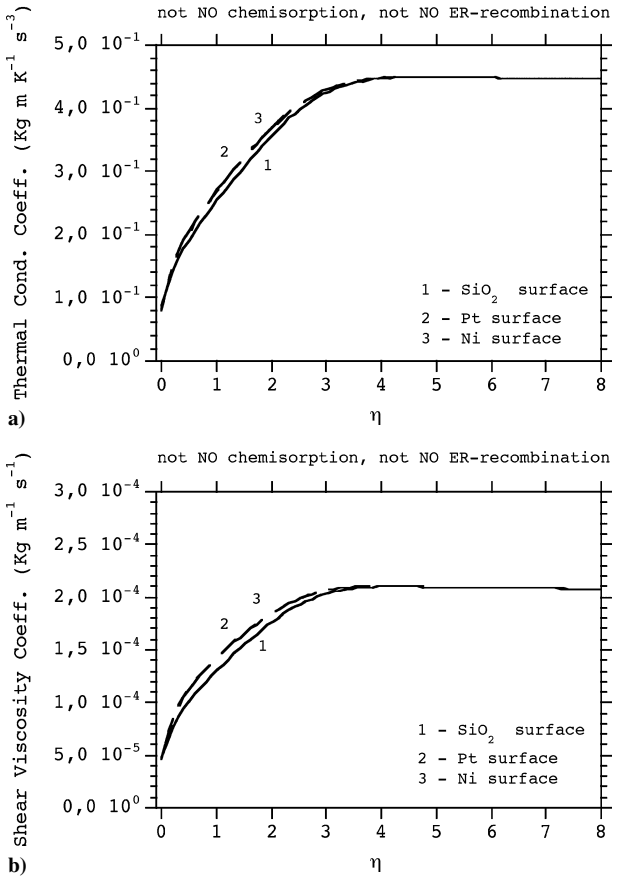

Fig. 8 Thermal conductivity coefficients (a) and shear viscosity coefficients (b) along η for different surfaces.

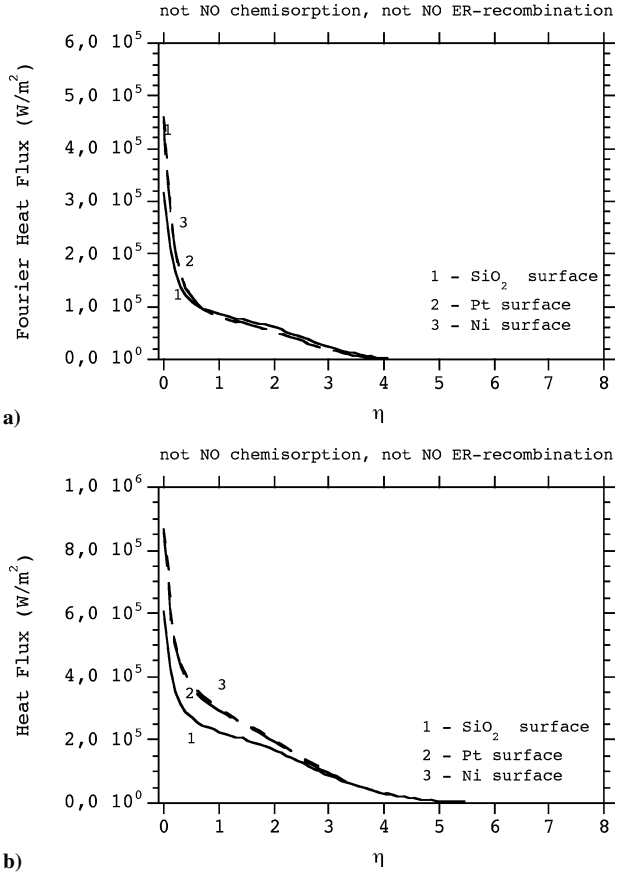

Fig. 9 Fourier heat flux (a) and total heat flux (b) along η for different surfaces.

gradient and the thermal conductivity coefficient trend, being proportional to their product [Eq. (37)]. The total heat flux includes both the Fourier heat flux and several diffusion terms [Eq. (36)], whereas the influence of the surface on the heat conduction is found to be weak, diffusion processes are strongly determined by the material catalytic properties. This is the reason for a considerable discrepancy between the total heat fluxes calculated near SiO_2 and metal surfaces. It is interesting to emphasize that the heat flux obtained at the SiO_2 surface is about 40–45% lower than the heat flux at the metal surfaces. Therefore, using SiO_2 surfaces provides lower thermal loads, which is important for reentry problems.

Contributions of various dissipative processes to the total heat flux are presented in Fig. 10. One can see that the values of the thermal diffusion flux (TD) and the flux due to vibrational energy diffusion (DVE) are approximately the same, although having opposite signs. Therefore, under conditions considered in the present study, these

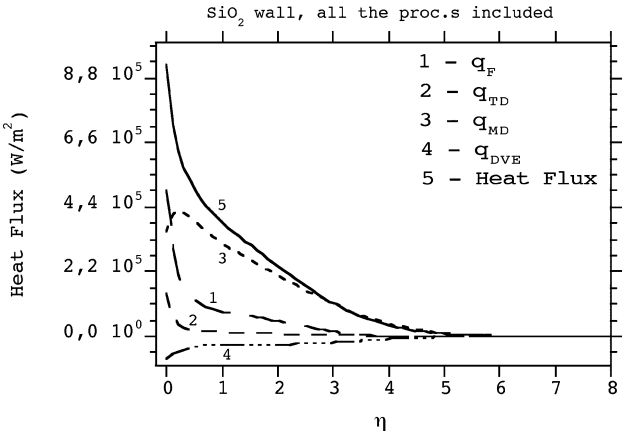

Fig. 10 Contributions of various dissipative processes to the total heat flux.

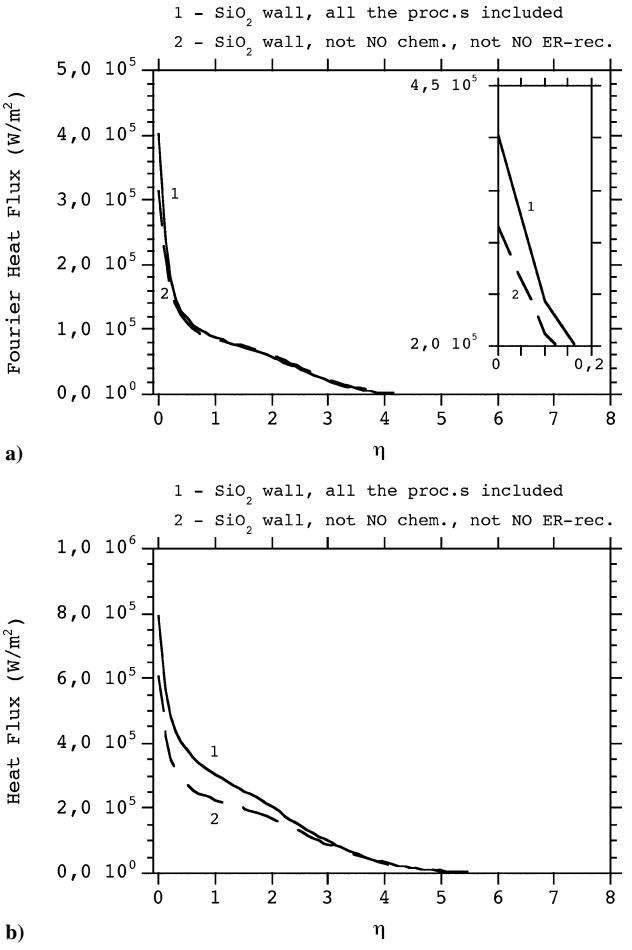

Fig. 11 Fourier heat flux (a) and total heat flux (b) along η for a SiO_2 surface.

two processes practically compensate for each other, and the main role in the heat transfer belongs to heat conduction and mass diffusion. The contribution of heat conduction is higher close to the wall, and decreases rapidly with distance from the surface. The role of mass diffusion is important in the whole region considered due to intensive reactive processes along the stagnation line. Thus, at $\eta > 1$, the total heat flux is determined mainly by the mass diffusion process.

It should be noted that the heat flux depends also on the interplay of numerous microscopic collision processes occurring in the gas phase and in the gas–surface interaction. The influence of VV, VT vibrational energy exchanges, surface and gas phase recombination, dissociation, and deactivation on the surface on the heat transfer was estimated in Refs. 27, 32, and 33. In the present paper, we study the effect of NO surface kinetics on the heat transfer. Because in the case of a SiO_2 surface we have a better knowledge of NO Eley–Rideal recombination and NO adsorption, we can compare the heat flux (Fourier and total) calculated inserting and neglecting these processes to the kinetics scheme. This comparison is reported in Figs. 11a and 11b. Inspection of this figure shows considerable difference in the results of two calculations, thus indicating the importance of including complete gas–surface interaction kinetics for the estimation of the heat flux. A similar difference is expected for the other surfaces.

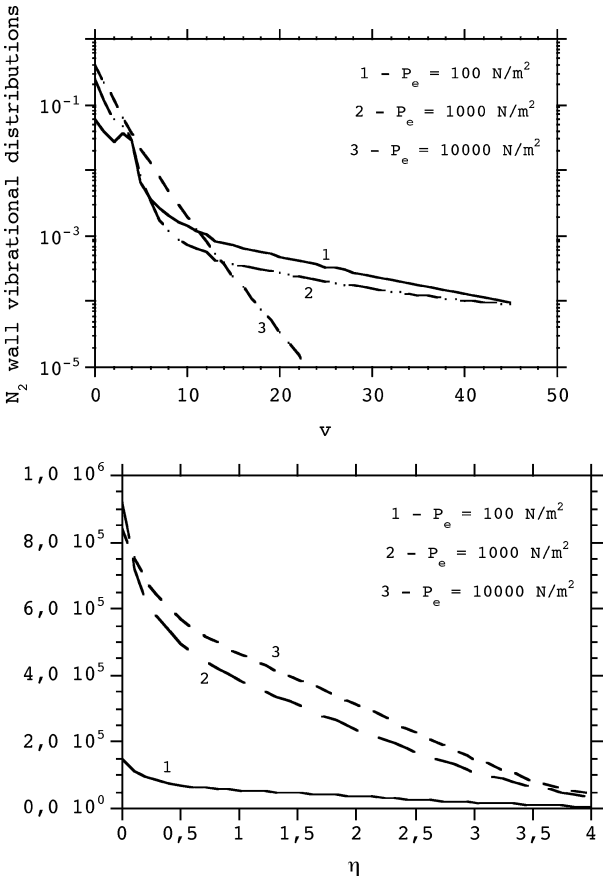

Fig. 12 N_2 (a) surface ($\eta = 0$) vibrational distributions vs vibrational level v and heat flux (b) vs η at different P_e, same conditions as the other figures for T_e, T_w, β.

The results thus far presented refer to typical reentry conditions. Calculations for SiO_2 obtained by changing the pressure in the boundary layer are reported in Figs. 12a and 12b. In particular, Fig. 12a reports the vibrational distributions of nitrogen near the surface, whereas Fig. 12b reports the heat flux in the boundary layer. We can see that the plateau in the nitrogen distribution disappears at high pressure because of the thermalization of the distributions by vT processes. On the other hand, the heat flux strongly increases on passing from 100 to 1000 N/m^2, having smaller consequences above 1000 N/m^2.

Validation of the present results suffers from the lack of dedicated experiments, which at the same time measure the nonequilibrium vibrational distributions and heat flux at the proper parameters in the boundary layer. A study is now in progress to compare the heat fluxes with the experimental ones at the stagnation point, even though we are aware that the heat flux values are in general not very sensitive to the details of the chemical–physical model.

IV. Conclusions

We have developed in the present paper a more realistic boundary layer model that simultaneously calculates the flowfield and the

surface recombination coefficients for hypersonic flows. The model represents a good solution to the problem of the mutual influence of the gas composition close to the surface and the surface recombination coefficients themselves.

The results emphasize the role of the catalyticity of different materials in the chemistry in the boundary layer of a reentering body. Metal surfaces show higher catalyticity and a larger effect on the boundary layer chemistry. Nonequilibrium vibrational distribution functions near the surface are observed as a result of both gas-phase and surface recombination. These distributions lead to generation of a nonmonotonic profile of the NO mass density along the boundary layer.

The surface catalyticity also influences the gas-phase transport properties, such as diffusion, thermal diffusion, thermal conductivity, shear viscosity coefficients, and Fourier and the total heat flux.

Appendix

The rate constant of each elementary kinetic process (1)–(14) can be expressed in the classical Arrenhius form[14,28]

$$k_i = B_i * e^{-E_i/RT}$$

where the preexponential B_i is the frequency factor and E_i is the activation energy of the ith process. Actually the rate constant assumes different forms depending on the preexponential factors and on what is possible to neglect. In the following the rates constants of processes (1)–(14) have been reported:

Processes (1, 2):

$$k_{\text{ch}}^{A} = S_{\text{A}} \times \sqrt{\frac{k_b T}{2\pi m_{\text{A}}}} \times \frac{1}{[S_0]}$$

with, if A = N, O on a Cu, Pt, Ni surface, $s_{\text{A}} = \bar{S}_{0\text{A}}$, for $T < T_{0\text{A}}$, and $s_{\text{A}} = \bar{S}_{0\text{A}} \times e^{(-\beta_{\text{A}}(T - T_{0\text{A}}))}$ for $T >= T_{0\text{A}}$.

Processes (3, 4, 5),

$$k_{\text{chdm}}^{A} = s_{\text{A}} \times \sqrt{\frac{k_b T}{2\pi m_{\text{A}}}} \times \frac{1}{[S_0]^2}$$

On an SiO_2 surface, $s_{\text{A}} = P_{\underline{\text{A}}} \times e^{-E_{a\text{A}}/k_b T}$; on a Cu, Pt, Ni surface, $s_{\text{A}} = \bar{S}_{0\text{A}}$ for $T < T_{0\text{A}}$, $s_{\text{A}} = \bar{S}_{0\text{A}} \times e^{(-\beta_{\text{A}}(T - T_{0\text{A}}))}$ for $T >= T_{0\text{A}}$, with A = N_2, O_2, NO.

Processes (6, 7, 8, 9):

$$k_{\text{ER}}^{\text{AB}} = \gamma'_{\text{AB}} \times \sqrt{\frac{k_b T}{2\pi m_{\text{A}}}} \times \frac{1}{[S_0]}$$

on an SiO_2 surface, with $\gamma'_{\text{AB}} = P_{\text{ER}}^{\text{AB}} \times e^{-O_{\text{ER}}^{\text{AB}}/k_b T}$,

$$k_{\text{ER}}^{\text{AB}} = P_{0r\text{AB}} \times \sqrt{\frac{k_b T}{2\pi m_{\text{A}}}} \times \frac{1}{[S_0]}$$

on a Cu, Pt, Ni surface, with $P_{0r\text{AB}} = \bar{\alpha}_{r\text{AB}}$ for $T < T_{0r\text{AB}}$ and $P_{0r\text{AB}} = \bar{\alpha}_{r\text{AB}} \times e^{(-\beta_{r\text{AB}}(T - T_{0r\text{AB}}))}$ for $T >= T_{0r\text{AB}}$ with A = N, O; B = N, O.

Processes (10, 11, 12):

$$k_{\text{LH}}^{\text{AB}} = \frac{1}{2}\left(\frac{C_{\text{A}}}{\Delta}\sqrt{\frac{\pi k_b T}{2m_{\text{A}}}} + \frac{C_{\text{B}}}{\Delta}\sqrt{\frac{\pi k_b T}{2m_{\text{B}}}}\right) \times e^{-Q_{\text{LH}}^{\text{AB}}/k_b T}\frac{1}{[S_0]}$$

on an SiO_2 surface, with $Q_{\text{LH}}^{\text{AB}} = Q_{a\text{A}} + Q_{a\text{B}} - E_{\text{AB}}$,

$$k_{\text{LH}}^{\text{AB}} = \frac{1}{2}\left(d_{\text{A}}\sqrt{\frac{\pi k_b T}{2m_{\text{A}}}} + d_{\text{B}}\sqrt{\frac{\pi k_b T}{2m_{\text{B}}}}\right) \times e^{-E_4/RT}$$

on a Cu, Pt, Ni surface, with $E_4 = E_{\text{A-M}} + E_{\text{B-M}} - E_{\text{A-B}}$), with A = N, O, B = N, O,

Processes (13, 14): on a SiO_2 surface,

$$k_{\text{td}}^{\text{A}} = \frac{k_b T}{h} \times e^{-Q_{a\text{A}}/k_b T}$$

on a Cu, Pt, Ni surface,

$$k_{\text{td}}^{\text{A}} = \frac{k_b T}{h} \times e^{-E_5/RT}$$

with $E_5 = E_{\text{A-M}}$ and with A = N, O.

In all of these formula, $E_{\text{N-N}} = 945$ KJ/mol, $E_{\text{O-O}} = 498$ KJ/mol, $E_{\text{NO}} = 625.1$ KJ/mol, $d_{\text{N}} = 70 \times 10^{-12}$ m, $d_{\text{O}} = 66 \times 10^{-12}$ m. The values of the other parameters appearing in this rate constants,

Table A1 Coefficients to calculate the rate constants on SiO_2

Coefficients	SiO_2
s_{N}	0.015
s_{O}	0.05
P_{N_2}	[a]
P_{O_2}	[a]
P_{NO}	[a]
$E_{a\text{N}_2}$	[a]
$E_{a\text{O}_2}$	[a]
$E_{a\text{NO}}$	[a]
$P_{\text{ER}}^{\text{NN}}$	0.1
$P_{\text{ER}}^{\text{OO}}$	0.1
$P_{\text{ER}}^{\text{NO}}$	0.1
$P_{\text{ER}}^{\text{ON}}$	0.1
$Q_{\text{ER}}^{\text{NN}}$	20 KJ/mol
$Q_{\text{ER}}^{\text{OO}}$	20 KJ/mol
$Q_{\text{ER}}^{\text{NO}}$	20 KJ/mol
$Q_{\text{ER}}^{\text{ON}}$	20 KJ/mol
$E_{m\text{N}}$	82.2 KJ/mol
$E_{m\text{O}}$	159.1 KJ/mol
c_{N}	0.0
c_{O}	0.0
Δ	5.0×10^{10} m
$Q_{a\text{N}}$	530.8 KJ/mol
$Q_{a\text{O}}$	499.8 KJ/mol

[a]Chemisorption of N_2, O_2, and NO, on SiO_2 can be neglected.

Table A2 Coefficients to calculate the rate constants on metal surfaces

Coefficients	Pt	Cu	Ni
$\bar{S}_{0\text{N}}$	0.55	0.55	0.45
$\bar{S}_{0\text{O}}$	0.45	0.8	0.6
β_{N}	0.0002	0.00025	0.0005
β_{O}	0.0001	0.00045	0.0005
$T_{\emptyset\text{N}}$	400	300	500
$T_{\emptyset\text{O}}$	400	300	500
$\bar{S}_{0\text{N}_2}$	[a]	[a]	[a]
$\bar{S}_{0\text{O}_2}$	0.2	0.4	0.3
$\bar{S}_{0\text{NO}}$	[a]	[a]	[a]
$T_{\emptyset\text{N}_2}$	[a]	[a]	[a]
$T_{\emptyset\text{O}_2}$	400	300	500
$T_{\emptyset\text{NO}}$	[a]	[a]	[a]
β_{N_2}	[a]	[a]	[a]
β_{O_2}	0.0005	0.0006	0.0005
β_{NO}	[a]	[a]	[a]
$\bar{\alpha}_{r\text{NN}}$	0.23	0.2	0.057
$\bar{\alpha}_{r\text{OO}}$	0.0055	0.085	0.01
$\bar{\alpha}_{r\text{NO}}$	0.23	0.2	0.057
$\bar{\alpha}_{r\text{ON}}$	0.0055	0.085	0.01
$T_{\emptyset r\text{NN}}$	400	300	500
$T_{\emptyset r\text{OO}}$	400	300	500
$T_{\emptyset r\text{NO}}$	400	300	500
$T_{\emptyset r\text{ON}}$	400	300	500
$\beta_{r\text{NN}}$	0.0001	0.0001	0.000095
$\beta_{r\text{OO}}$	0.0005	0.0002	0.0007
$\beta_{r\text{NO}}$	0.0001	0.0001	0.000095
$\beta_{r\text{ON}}$	0.0005	0.0002	0.0007
$E_{m\text{N}}$	?	?	?
$E_{m\text{O}}$	?	?	?
$E_{\text{N-M}}$	605 KJ/mol	560 KJ/mol	602.5 KJ/mol
$E_{\text{O-M}}$	344 KJ/mol	309 KJ/mol	354 KJ/mol

Note: ? = data missing.
[a]Assumption: N_2 and NO cannot be chemisorbed by Cu, Pt, or Ni.

for the different surface materials here considered, are reported in Tables A1 and A2.

Acknowledgments

This work has been partially supported by ASI-CAST and by Prin 2003 No. 2003037912_010 (Dinamica molecolare di processi elementari in condizioni di non-equilibrio).

References

[1]Greaves, J. C., and Linnett, J. W., "The Recombination of Oxygen Atoms at Surfaces," *Transactions of the Faraday Society*, Vol. 54, 1958, pp. 1323–1330.

[2]Fay, J. A., and Riddell, F. R., "Theory of Stagnation Point Heat Transfer in Dissociated Air," *Journal of the Aeronautical Sciences*, Vol. 25, No. 2, 1958, pp. 73–85.

[3]Goulard, R., "On Catalytic Recombination Rates in Hypersonic Stagnation Heat Transfer," *Jet Propulsion*, Vol. 28, No. 11, 1958, pp. 737–745.

[4]Halpern, B., and Rosner, D. E., "Chemical Energy Accomodation at Catalyst Surfaces," *Chemical Society, Faraday Transactions I*, Vol. 74, 1978, pp. 1833–1912.

[5]Halpern, B., and Rosner, D. E., "Incomplete Energy Accomodation in Surface-Catalyzed Reactions," *Heterogeneous Atmospheric Chemistry*, Geophysical Monograph Series, Vol. 26, edited by D. R. Schryer, American Geophysical Union, Washington, DC, 1982, pp. 167–171.

[6]Scott, C. D., "Catalytic Recombination of Nitrogen and Oxygen on High-Temperature Reusable Surface Insulation," *Aerothermodynamics and Planetary Entry*, edited by A. L. Crosbie, Progress in Astronautics and Aeronautics, Vol. 77, AIAA, New York, 1980, pp. 193–212.

[7]Stewart, D. A., Rakich, J. V., and Lanfranco, M. J., "Catalytic Surface Effects Experiment on the Space Shuttle," *Thermophysics of Atmospheric Entry*, Progress in Astronautics and Aeronautics, Vol. 82, AIAA, New York, 1982, pp. 248–272.

[8]Kolodziej, P., and Stewart, D. A., "Nitrogen Recombination on High-Temperature Reusable Surface Insulation and the Analysis of its Effects on Surface Catalysis," AIAA Paper 87-1637, June 1987.

[9]Stewart, D. A., Chen, Y. K., and Henline, W. D., "Effect of Non-equilibrium Flow Chemistry and Surface Catalysis on Surface Heating to AFE," AIAA Paper 91-1373, June 1991.

[10]Carleton, K. L., and Marinelli, W. J., "Spececraft Thermal Energy Accomodation from Atomic Recombination," *Journal of Thermophysics and Heat Transfer*, Vol. 6, No. 4, 1992, pp. 650–655

[11]Zoby, E. V., Gupta, R. N., Jr., and Simmonds, A. L., "Temperature-Dependent Reaction-Rate Expression for Oxygen Recombination at Shuttle Entry Conditions," AIAA Paper 1984-224, Jan. 1984.

[12]Seward, W. A., and Jumper, E. J., "Model for Oxygen Recombination on Silicon-Dioxide Surfaces," *Journal of Thermophysics and Heat Transfer*, Vol. 5, No. 3, 1991, pp. 284–291.

[13]Jumper, E. J., Newman, M., Seward, W. A., and Kitchen, D. R., "Recombination of Nitrogen on Silica-Based, Thermal-Protection-Tile-Like Surfaces," AIAA Paper 93-0477, Jan. 1993.

[14]Nasuti, F., Barbato, M., and Bruno, C., "Material-Dependent Catalytic Recombination Modeling for Hypersonic Flows," *Journal of Thermophysics and Heat Transfer*, Vol. 10, No. 1, 1996, pp. 131–136.

[15]Daiss, A., Fruhauf, H. H., and Messerschmid, E. W., "Chemical Reactions and Thermal Nonequilibrium on Silica Surface," *Molecular Physics and Hypersonic Flows*, edited by M. Capitelli, NATO-ASI Series, Vol. C-482, Kluwer Academic, 1996, pp. 203–218.

[16]Kurotaki, T., "Construction of Catalytic Model on SiO2-Based Surface and Application on Real Trajectory," AIAA Paper 2000-2366, June 2000.

[17]Barbato, M., and Bruno C., "Heterogeneous Catalysis: Theory, Models and Applications," *Molecular Physics and Hypersonic Flows*, edited by M. Capitelli, Kluwer Academic, Norwell, MA, 1996, pp. 139–160.

[18]Copeland, R. A., Pallix, J. B., and Stewart, D. A., "Surface-Catalyzed Production of NO from Recombination of N and O Atoms," *Journal of Thermophysics and Heat Transfer*, Vol. 12, No. 4, 1998, pp. 496–499.

[19]Armenise, I., Capitelli, M., Gorse, C., Cacciatore, M., and Rutigliano, M., "Nonequilibrium Vibrational Kinetics of a O_2/O Mixture Hitting a Catalytic Surface," *Journal of Spacecraft and Rockets*, Vol. 37, No. 3, 2000, pp. 318–323; also AIAA Paper 99-3631, June–July 1999.

[20]Cacciatore, M., Rutigliano, M., and Billing, G. D., "Eley–Rideal and Langmuir–Hinshelwood Recombination Coefficients for Oxygen on Silica Surfaces," *Journal of Thermophysics and Heat Transfer*, Vol. 13, No. 2, 1999, pp. 195–203.

[21]Capitelli, M., Armenise, I., and Gorse, C., "State-to-State Approach in the Kinetics of Air Components Under Re-Entry Conditions," *Journal of Thermophysics and Heat Transfer*, Vol. 11, No. 4, 1997, pp. 570–578.

[22]Armenise, I., Capitelli, M., and Gorse, C., "Nitrogen Nonequilibrium Vibrational Distributions and Non-Arrhenius Dissociation Constants in Hypersonic Boundary Layers," *Journal of Thermophysics and Heat Transfer*, Vol. 12, No. 1, 1998, pp. 45–51.

[23]Armenise, I., Capitelli, M., and Gorse, C., "Non-Equilibrium Vibrational Kinetics of Air Hitting a Catalytic SiO_2 Surface," *Journal of Spacecraft and Rockets*, Vol. 38, No. 4, 2001, pp. 482–487.

[24]Armenise, I., and Capitelli, M., "State to State Vibrational Kinetics in the Boundary Layer of Entering Body in Earth Atmosphere: Particle Distributions and Chemical Kinetics," *Plasma Sources Science and Technology*, Vol. 14, No. 2, 2005, pp. S9–S17.

[25]Armenise, I., Barbato, M., Capitelli, M., and Gorse, C., "Surface Recombination Coefficients and Boundary-Layer Hypersonic-Flows Calculations on Different Surfaces," *Journal of Spacecraft and Rockets*, Vol. 41, No. 2, 2004, pp. 310–313.

[26]Kustova, E. V., "On the Simplified State-to-State Transport Coefficients," *Chemical Physics*, Vol. 270, No. 1, 2001, pp. 177–195.

[27]Armenise, I., Capitelli, M., and Kustova, E. V., "State-to-State Kinetics and Transport Properties of a Reactive Air Flow Near a Re-entering Body Surface," *Proceedings of 24th RGD Conference*, edited by M. Capitelli, AIP, Melville, NY, 2005, pp. 1061–1066.

[28]Barbato, F. M., Reggiani, S., Bruno, C., and Muylaert, J., "Model for Heterogeneous Catalyis on Metal Surfaces with Applications to Hypersonic Flows," *Journal of Thermophysics and Heat Transfer*, Vol. 14, No. 3, 2000, pp. 412–420.

[29]Doroshenko, V. M., Koudriatsev, N. N., Novikov, S. S., and Smetanin, V. V., "Dependence of Heat Transfer on the Formation of Vibrationally Excited Nitrogen Molecules During the Recombination of Atoms in a Boundary Layer," *High Temperature*, Vol. 28, No. 1, 1990, pp. 70–76.

[30]Anderson, J. D., Jr., *Hypersonic and High Temperature Gas Dynamics*, McGraw–Hill Series in Aeronautical and Aerospace Engineering, McGraw–Hill, New York, 1989, pp. 213–259, 611–636.

[31]Kustova, E. V., and Nagnibeda, E. A., "Transport Properties of a Reacting Gas Mixture with Strong Vibrational and Chemical Nonequilibrium," *Chemical Physics*, Vol. 233, No. 1, 1998, pp. 57–75.

[32]Armenise, I., Capitelli, M., Kustova, E. V., and Nagnibeda, E. A., "The Influence of Nonequilibrium Kinetics on the Heat Transfer and Diffusion near Re-Entering Body," *Journal of Thermophysics and Heat Transfer*, Vol. 13, No. 2, 1999, pp. 210–218.

[33]Kustova, E. V., Nagnibeda, E. A., Armenise, I., and Capitelli, M., "Nonequilibrium Kinetics and Heat Transfer in O_2/O Mixtures near Catalytic Surfaces," *Journal of Thermophysics and Heat Transfer*, Vol. 16, No. 2, 2002, pp. 238–244.

[34]Ferziger, J. H., and Kaper, H. G., *Mathematical Theory of Transport Processes in Gases*, North-Holland, Amsterdam, 1972, p. 175.